Physics Letters B 802 (2020) 135249

Contents lists available at ScienceDirect

Physics Letters B

www.elsevier.com/locate/physletb

Study of the nuclear symmetry energy from the rapidity-dependent elliptic flow in heavy-ion collisions around 1 GeV/nucleon regime

Yongjia Wang [a], Qingfeng Li [a,b,*], Yvonne Leifels [c], Arnaud Le Fèvre [c]

[a] School of Science, Huzhou University, Huzhou 313000, China
[b] Institute of Modern Physics, Chinese Academy of Sciences, Lanzhou 730000, China
[c] GSI Helmholtzzentrum für Schwerionenforschung GmbH, D-64291 Darmstadt, Germany

ARTICLE INFO

Article history:
Received 3 December 2019
Received in revised form 13 January 2020
Accepted 16 January 2020
Available online 22 January 2020
Editor: W. Haxton

Keywords:
Nuclear symmetry energy
Transport model
Heavy ion collision
Elliptic flow

ABSTRACT

The elliptic flow ratio of neutrons versus protons in heavy-ion collisions (HICs) is one of the important probes to constrain the nuclear symmetry energy, however measuring the flow of neutrons with high precision is a great challenge for experimental techniques. In this work, the elliptic flow of protons is studied and it is found that the rapidity at which the sign of v_2 changes from negative to positive is sensitive to the density dependence of the symmetry energy. By comparing the existing FOPI experimental data for proton flows to the calculations with the ultrarelativistic quantum molecular dynamics (UrQMD) model, the slope parameter of the nuclear symmetry energy is extracted to be $L_0 = 43 \pm 20$ MeV at 95% confidence level. This is in good agreement with many recent results from investigations of nuclear structure properties and also partly overlaps with the recent result of the ASY-EOS experiment.

The nuclear symmetry energy $E_{\rm sym}$ is essential for our understanding of diverse phenomena observed in rare isotopes, nuclear reactions with exotic nuclei, as well as neutron star mergers [1–10]. To determine how the symmetry energy evolves with nuclear density has attracted considerable attention in recent two decades. It is also one of the important goals of the current and future rare isotope beam facilities (e.g., the FRIB at MSU in the United States, the RIBF at RIKEN in Japan, the SPIRAL2 at GANIL in France, the CSR at HIRFL and the HIAF in China, FAIR in Germany and so on) around the world. In recent several years, great efforts have been made to determine parameters (e.g., the coefficient $S_0 = E_{\rm sym}(\rho_0)$ and the slope $L_0 = 3\rho_0 \left(\frac{\partial E_{\rm sym}(\rho)}{\partial \rho}\right)|_{\rho=\rho_0}$) of the symmetry energy at saturation density (ρ_0), but a complete picture of the $E_{\rm sym}$ as a function of nuclear density has still not emerged (see, e.g., Refs. [11–31]).

Heavy-ion collisions (HICs) at beam energies of several hundreds MeV/nucleons permit creating nuclear matter with density and isospin asymmetry from their normal values. It is also a unique way to form nuclear matter with high density and isospin asymmetry on earth. Usually, final observables in experiments of HICs are compared to simulations of transport models for the purpose of deducing properties of the created nuclear matter. Particle (such as, protons and neutrons, pions, kaons, etc.) multiplicities and collective flows (the directed flow and elliptic flow) are the most commonly used observables in HICs at intermediate energies (several hundreds MeV per nucleon). Probably one of the best-known example in HICs at intermediate energies is the determination of the incompressibility K_0 of the isospin symmetric nuclear matter by comparing the experimental data of collective flow and kaon yield with transport model calculations [32,33].

To study the density dependence of the nuclear symmetry energy using HICs, several sensitive observables have been presented, such as the yield ratio between isospin partners (neutrons and protons, ^{3}H and ^{3}He, π^- and π^+, K^+ and K^0, etc.), and the elliptic flow ratio of neutrons versus protons v_2^n/v_2^p. In spite of the progress made, a tighter constraint on the nuclear symmetry energy at high density is still very difficult to achieve due to a) the difficulties in precision experimental measurements, and b) strong model- and observable-dependent results, see, e.g., Refs. [34–37]. Thus, finding new observables which are sensitive to the $E_{\rm sym}(\rho)$ is absolutely needed.

In this paper, by studying the rapidity-dependent elliptic flow of protons produced in heavy-ion collisions in the 1 GeV/nucleon regime, a new observable reflecting the rapidity at which the sign of elliptic flow changes from negative to positive, is found to be

* Corresponding author at: School of Science, Huzhou University, Huzhou 313000, China.
E-mail address: liqf@zjhu.edu.cn (Q. Li).

https://doi.org/10.1016/j.physletb.2020.135249

sensitive to the $E_{\rm sym}(\rho)$. Comparing the FOPI experimental data to simulations with the ultrarelativistic quantum molecular dynamics (UrQMD) model, a preferred range of slope parameter L_0 is extracted.

In the present version of the UrQMD model, the total Hamiltonian consists of the kinetic energy, the Coulomb potential energy, the local potential energy, and the non-local potential energy. The local term is derived from the integration of the Skyrme potential energy density functional [38,39]. The non-local term $V_{md} = 1.57[\ln(500(\Delta p)^2 + 1)]^2\rho/\rho_0$ [40] which has been widely used in QMD-like models is also considered. In this case, the effective masses of neutron and proton are the same in the present version of UrQMD model. With an isospin-dependent form of V_{md} will give rise to the issues of the momentum dependence of the symmetry potential and the associated neutron-proton effective mass splitting [5,41]. Effect of the neutron-proton effective mass splitting on the elliptic flow has been studied with various models, but still with some puzzling inconsistency [42–47]. To compare with constraints on the nuclear symmetry energy obtained with the elliptic flow ratio of free neutrons verse hydrogen isotopes in Refs. [21,23,24] and that with observable used in this work, the isospin-independent form of the momentum dependent potential is still incorporated the same as that in Refs. [21,23,24]. In addition, the effect of the neutron-proton effective mass splitting on observables is expected to be suppressed at higher beam energies, because both the effective masses of proton and that of neutron approach the free mass at higher momentum. Therefore, an isospin-independent form of the momentum dependent potential is still considered as appropriate for the current analysis of elliptic flow. Together with proper parameter sets in the in-medium nucleon-nucleon cross section and the algorithm for cluster recognition, the recently published flow data of the FOPI Collaboration for light charged clusters [48,49] can be reproduced well [39,50]. In addition, with further considering the pion-nucleon and kaon-nucleon potentials, the collective flow of pions and kaons can also be well described [51,52].

With the introduction of the Skyrme potential energy density functional, ρ_0, K_0, S_0, and L_0 can not be varied independently. In order to isolate the influence of L_0 on observables from other effects, 11 Skyrme interactions Skz4, Skz2, Skz0, SV-mas08, SLy230a, SLy5, SV-sym32, MSL0, SV-sym34, Gs, and SkI1[53], for which give quite similar values of ρ_0 (within about 0.16 ± 0.002 fm^{-3}), K_0 (within about 235 ± 5 MeV), and S_0 (within about 32 ± 2 MeV), but different L_0 and K_{sym}, are selected strictly. To have a wider variation in L_0, SkI1 which gives larger values of $K_0 = 243$ MeV and $S_0 = 37.5$ MeV is also considered. The saturation properties of the selected forces are shown in Table 1. We note that the empirical linear correlation between L_0 and K_{sym} which has been found from many microscopic many-body theories and phenomenological models is also preserved for the selected 11 Skyrme interactions. Around a reference density ρ_r, the slope parameter can be written as $L(\rho_r) = 3\rho_r\left(\frac{\partial E_{\rm sym}(\rho)}{\partial\rho}\right)|_{\rho=\rho_r}$ which measures the density dependence of $E_{\rm sym}(\rho)$ around ρ_r. The nuclear symmetry energy $E_{\rm sym}(\rho)$, its slope $L(\rho)$, and the symmetry potential with $\delta = 0.2$ are shown as a function of nuclear density in Fig. 1. For comparison, recent constraints on the symmetry energy and its slope parameter at subsaturation densities are also displayed. It can be seen that these constraints on the slope parameters $L(\rho \approx 0.10)$ can be covered by the results predicted with SV-mas08, SLy230a, SLy5, SV-sym32, and MSL0, while the $L(\rho \approx 0.10)$ obtained with the two soft cases (i.e., Skz4 and Skz2) and three stiff cases (i.e., SV-sym34, Gs, and SkI1) are far from those constraints. The $E_{\rm sym}(\rho)$ obtained with SLy230a, SLy5, SV-sym32, and MSL0 are quite close to each other for the density range of 0.2–0.32 fm^{-3} and also comparable with the recent constraint at $2\rho_0$ obtained from observations of neutron stars and gravitational waves [17,18], but their slopes $L(\rho)$ display remarkably diverse behaviors at higher density.

Table 1
Saturation properties of nuclear matter as obtained with selected Skyrme parameterizations used in this work.

	ρ_0 (fm^{-3})	K_0 (MeV)	S_0 (MeV)	L_0 (MeV)	K_{sym} (MeV)
Skz4	0.16	230	32.0	5.8	-240.9
Skz2	0.16	230	32.0	16.8	-259.7
Skz0	0.16	230	32.0	35.1	-242.2
SV-mas08	0.16	233	30.0	40.2	-172.4
SLy230a	0.16	230	32.0	44.3	-98.2
SLy5	0.16	230	32.0	48.2	-112.7
SV-sym32	0.159	234	32.0	57.1	-148.8
MSL0	0.16	230	30.0	60.0	-99.3
SV-sym34	0.159	234	34.0	80.9	-79.1
Gs	0.158	237	31.1	93.3	14.1
SkI1	0.16	243	37.5	161.1	234.7

With the parabolic approximation, the equation-of-state (EOS) of isospin asymmetric nuclear matter can be generally expressed as $E(\rho,\delta) = E_0(\rho,0) + E_{\rm sym}(\rho)\delta^2$, here $\delta = (\rho_n - \rho_p)/(\rho_n + \rho_p)$ is the isospin asymmetry, E_0 is the energy per nucleon for symmetric nuclear matter. Then the pressure in the isospin asymmetric nuclear matter is proportional to the slope of the symmetry energy [56], $P(\rho,\delta) = \rho^2\frac{\partial E}{\partial\rho} = \rho^2\frac{\partial E_0(\rho)}{\partial\rho} + \frac{1}{3}\rho L(\rho)\delta^2$. It is known from the fluid mechanics, the collective motion of nucleons is directly connected to the pressure gradients in x-, y-, and z-directions [54,55]. On one hand, one may expect that observables are directly connected to the pressure gradients, then to $K_{sym} = 3\rho_0\left(\frac{\partial L(\rho)}{\partial\rho}\right)|_{\rho=\rho_0}$. On the other hand, the development and evolution of the elliptic flow in HICs at beam energies studied in this work is much more complicated than the fluid dynamics, it does not only depend on the pressure gradient but also affected by the blocking of the spectators. Thus, an intimate connection between K_{sym} and the elliptic flow (ratio between neutrons and protons) may not necessarily be observed.

The elliptic flow is one of the most common used observables in HICs with incident energy from several hundreds of MeV/nucleon up to the highest energies presently available at LHC/CERN. It is the second-order coefficient in the Fourier expansion of the azimuthal distribution of emitted particles, $v_2 = \left\langle\frac{p_x^2 - p_y^2}{p_t^2}\right\rangle$. Here, p_x and p_y are the two components of the transverse momentum $p_t = \sqrt{p_x^2 + p_y^2}$, and the angular bracket denotes an average over all considered particles of all events. Usually, v_2 has a complex multi-dimensional structure. For a certain species of particles produced in a nuclear reaction with fixed colliding system, beam energy, and impact parameter, v_2 depends both on the rapidity y_z and the transverse momentum p_t. The scaled units $y_0 \equiv y/y_{1cm}$ and $u_{t0} \equiv u_t/u_{1cm}$ (the transverse component of the four-velocity, the subscript $1cm$ denotes the incident projectile in the center-of-mass system) are used instead of y_z and p_t throughout, in the same way as done in the experimental report [49], in order to scale with whole incident energies.

To see more clearly effects of the nuclear symmetry energy on the elliptic flow v_2, the v_2 of free protons and neutrons calculated with the three parameter sets Skz4, SV-sym34, and SkI1 are shown in Fig. 2. It can be seen that the calculations for protons are in good agreement with the FOPI data in the whole inspected rapidity range, and that the v_2 as a function of rapidity y_0 can be well described by a quadratic fit $v_2 = v_{20} + v_{22}\cdot y_0^2$ [57]. Apparently, v_{20} represents the elliptic flow at mid-rapidity which has attracted a lot of interest in the heavy-ion community. And, the

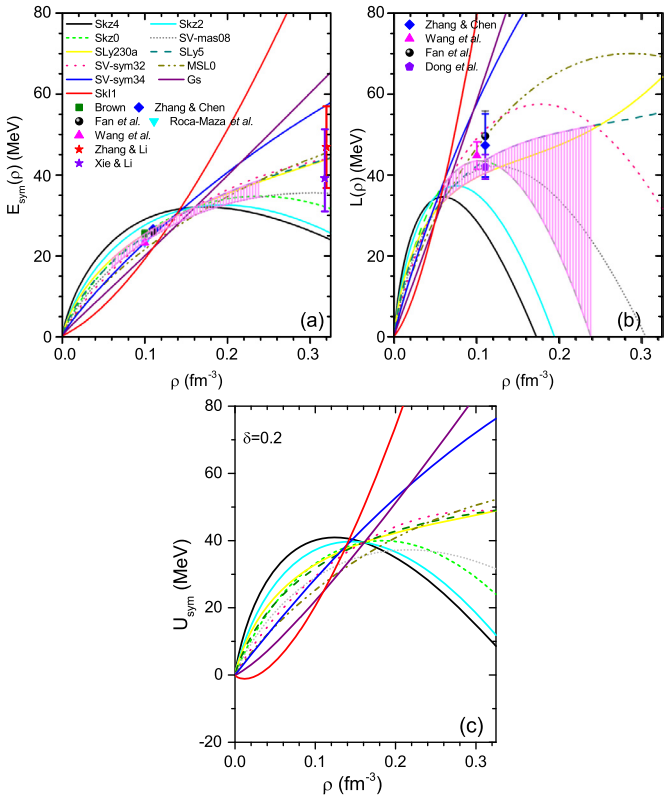

Fig. 1. The nuclear symmetry energy $E_{sym}(\rho)$ [panel (a)], its slope $L(\rho)$ [panel (b)], and the symmetry potential with $\delta = 0.2$ [panel (c)] are plotted as a function of density. The various lines show predictions for the selected 11 Skyrme interactions. Different scattered symbols represent recent constraints obtained by Roca-Maza et al. [11], Zhang and Chen [12], Brown [13], Fan et al. [14], Dong et al. [15], Wang et al. [16], Zhang and Li [17], and Xie and Li [18], respectively. Shaded bands represent the region covered by Skz0, SV-mas08, SLy230a, and SLy5.

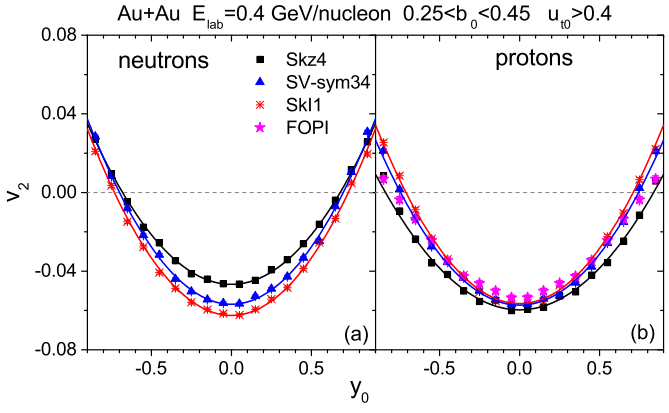

Fig. 2. The elliptic flow v_2 of free neutrons (a) and protons (b) produced from Au+Au collisions at 0.4 GeV/nucleon with centrality $0.25 < b_0 < 0.45$ and transverse velocity $u_{t0} > 0.4$, as a function of the normalized rapidity y_0. Calculations with Skz4 (solid square), SV-sym34 (solid triangle), and SkI1 (asterisk) are shown and compared with the FOPI data for free protons (solid star) reported in Ref. [49]. Solid lines are fits to the calculated results assuming $v_2(y_0) = v_{20} + v_{22} \cdot y_0^2$.

transition rapidity $y_t = \pm\sqrt{\frac{-v_{20}}{v_{22}}}$ represents the rapidity at which the v_2 changes sign from positive to negative. The v_{20} of free neutrons is very sensitive to the nuclear symmetry energy, and its absolute value calculated with SkI1 (stiff symmetry energy) is larger than that with Skz4 (soft symmetry energy), while the v_{20} of free protons shows a relatively weak dependence on the symmetry energy; its absolute value is larger in the case of Skz4. The

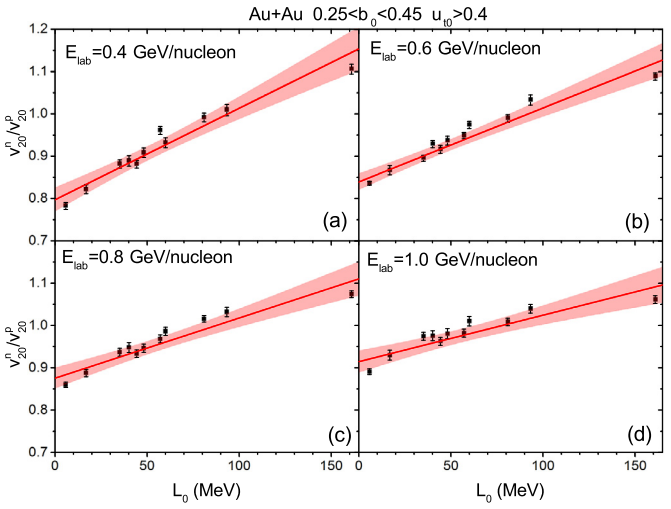

Fig. 3. The ratio between the elliptic flow parameter of free neutrons and protons v_{20}^n/v_{20}^p are plotted as a function of the slope parameter L_0. Calculations with the 11 Skyrme interactions are shown by solid symbols. The solid lines represent linear fits to the calculations, shaded bands are 95% confidence intervals around the fitted lines.

opposite influence of the symmetry energy on the v_{20} of protons and neutrons has been reported and discussed in Refs. [21–23, 27–29], it can be understood from the fact that the symmetry potential tends to expel neutrons and attract protons in a neutron-rich environment. The repulsion and attraction are stronger for the stiff symmetry energy at densities above ρ_0. Clearly, the v_{20} ratio between neutrons and protons v_{20}^n/v_{20}^p can be taken as a promising observable for constraining the nuclear symmetry energy at high density and has been used for that purpose [21–23,27–29]. It is known from previous studies that taking the ratio is better than taking the difference between neutrons and protons, because the impact from uncertainties in the isoscalar components (e.g., the incompressibility of the isospin symmetric matter and the in-medium nucleon-nucleon cross section) can be largely cancelled out [21,23]. In addition, the uncertainty associated with the reconstruction of the reaction plane in experiment also can be cancelled by taking the ratio [21,24].

Fig. 3 shows the v_{20}^n/v_{20}^p from Au+Au collisions at beam energies of 0.4, 0.6, 0.8, and 1.0 GeV/nucleon calculated with the 11 Skyrme interactions. A fairly linear relationship between the v_{20}^n/v_{20}^p and L_0 can be noticed, confirming that the v_{20}^n/v_{20}^p is indeed sensitive to the nuclear symmetry energy. The slope of the fitted line gradually decreases with increasing beam energy, due to mean field effects being weakened in more violent collisions occurring at higher energies. In addition, neutrons (protons) can be converted to protons (neutrons) through inelastic collisions (e.g., $n + n \to p + \Delta^- \to p + n + \pi^-$), thereby further reducing the effects of the symmetry energy on the flow of nucleons. Precise and systematic experimental measurements of the v_{20}^n/v_{20}^p from different colliding systems and beam energies would allow a more reliable constraint on the nuclear symmetry energy. Though the elliptic flow of neutrons has been measured by ASY-EOS collaboration with the Large Area Neutron Detector (LAND) [21,24], a systematic high-precision measurement of the flow of neutrons at various systems and beam energies is still a great challenge for experimental techniques to date.

We observe in Fig. 2 that the transition rapidity y_t is affected by the nuclear symmetry energy. The y_t of protons calculated with a soft symmetry energy (i.e., Skz4) is larger than that with a stiff symmetry energy (i.e., SkI1), while the trend for neutrons, even though weaker, is reversed. A stronger repulsive residual in-

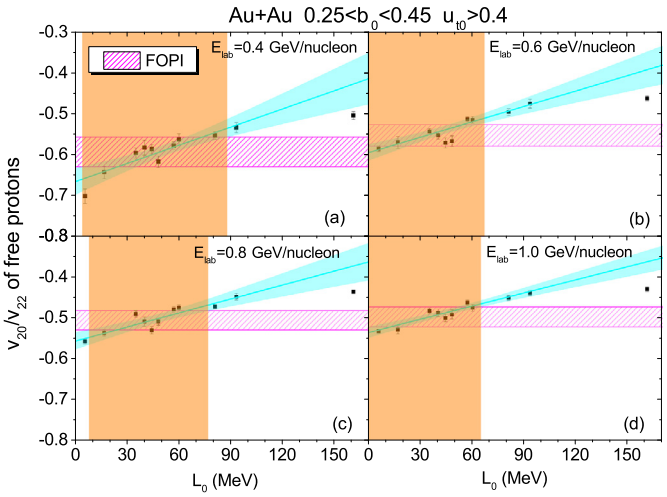

Fig. 4. The ratio v_{20}/v_{22} of free protons are shown as a function of the slope parameter L_0. Calculations with the selected 11 Skyrme interactions are shown by solid symbols. The horizontal bands represent the FOPI experimental data [49]. The solid lines represent linear fits to the calculations (except the results obtained from the stiffest symmetry energy, i.e., SkI1), cyan shaded bands are 95% confidence intervals around the fitted lines. The intersections of the horizontal bands and cyan shaded bands yield the width of the vertical orange bands, which constrain the slope L_0.

teraction (i.e., SkI1 for neutrons and Skz4 for protons) leads to a stronger squeeze out effect, it results in a larger value of transition rapidity y_t.

Fig. 4 shows the ratio v_{20}/v_{22} of free protons produced from Au+Au collisions at beam energies of 0.4, 0.6, 0.8, and 1.0 GeV/nucleon. A strong degree of linearity between v_{20}/v_{22} and the slope parameter L_0 within the range 0 to 100 MeV can be observed. Clearly, v_{20}/v_{22} calculated with Gs and SkI1 (stiff symmetry energy with L_0 larger than 90 MeV) both fall outside the experimental intervals at four beam energies. The intersections of the FOPI data bands and calculated bands offer an opportunity to estimate the slope L_0, and $8 \leq L_0 \leq 65$ MeV is found out which fully meets all of the above four energies. The v_{20}/v_{22} calculated with Skz0, SV-mas08, SLy230a, and SLy5 are inside the experimental bands. The symmetry energy $E_{\rm sym}(\rho)$ as well as its slope $L(\rho)$ (shaded bands in Fig. 1) predicted by these four Skyrme parametrizations cover the constraintes obtained by Zhang et al. [12], Fan et al. [14], Dong et al. [15], and Wang et al. [16] from nuclear mass, electric dipole polarizability and neutron skin thickness, and the constraints obtained by Zhang and Li [17] and Xie and Li [18] from astrophysical observations. In addition, one may notice that the v_{20}/v_{22} calculated with these four interactions may not always increase with increasing L_0, as can be seen in Fig. 4 and more clearly in Fig. 7 where the excitation function of the v_{20}/v_{22} of free protons in Au+Au collisions is displayed. For example, the v_{20}/v_{22} calculated with the Skz0 ($L_0 = 35.1$ MeV, $K_{sym} = -242.2$ MeV) is larger than that with the SV-mas08 ($L_0 = 40.2$ MeV, $K_{sym} = -172.4$ MeV), SLy230a ($L_0 = 44.3$ MeV, $K_{sym} = -98.2$ MeV), and SLy5 ($L_0 = 48.2$ MeV, $K_{sym} = -112.7$ MeV). It may imply that both L_0 and K_{sym} are attributed to v_{20}/v_{22}.

The parameter v_{20} reflects the high density behavior of the nuclear symmetry energy as discussed in Fig. 2, while the parameter v_{22} is more likely to characterize the motion of particles around the target and projectile rapidities where the density is close to or even below the saturation density. To reveal this more clearly, we plot the correlation between density and rapidity at different reaction times in Figs. 5 and 6. At the initial time (two nucleons begin to contact each other), rapidities of nucleons are close to ± 1, and density is below the saturation density. As the projectile and target penetrate each other, the nucleon rapidity distribution and density distribution vary gradually and a high-density phase is created. The average density at mid-rapidity is larger than that at target/projectile rapidities, see e.g., the cases $t = 10$, 15, 20, and 25 fm/c in Fig. 5 at $E_{\rm lab} = 0.4$ GeV/nucleon, and the density distributions around target/projectile rapidities spread out, spanning a wider range of values, from almost zero to 0.4 fm^{-3}. Thus the collective-flow pattern of particles at mid-rapidity is influenced strongly by the high-density behavior of $E_{\rm sym}(\rho)$, while the motion of particles around target/projectile rapidities is more likely to be affected by the $E_{\rm sym}(\rho)$ at both subnormal and high densities. As can be seen in Fig. 7, the value of v_{20}/v_{22} varies from about -0.65 at $E_{\rm lab} =$ 0.4 GeV/nucleon to -0.45 at $E_{\rm lab} = 1.2$ GeV/nucleon, one obtains the transition rapidity $|y_t| = 0.7 \sim 0.8$. At the maximal compressed stage, i.e., about $t = 15$ fm/c at $E_{\rm lab} = 0.4$ GeV/nucleon and 9 fm/c at $E_{\rm lab} = 1.2$ GeV/nucleon, the averaged density around y_t are about 0.17 and 0.24 fm^{-3} at $E_{\rm lab} = 0.4$ and 1.2 GeV/nucleon, respectively. This provides a rough estimation of the maximal sensitive density for v_{20}/v_{22}. After 25 fm/c, the system undergoes a collective expansion and eventually the density is smaller than the saturation density. During the expansion, the momentary azimuthal distribution is continuing to evolve towards the asymptotic distribution which is characterized by v_{20} and v_{22} [57,58], under the governing of the nuclear potentials at subnormal densities. The effects of the symmetry potential on the v_{20}/v_{22} are then reduced. Since the potential becomes relatively weak at subnormal densities, the difference in v_{20}/v_{22} caused by different symmetry energy remains at final stage.

With increasing beam energy, more and more nucleons will be involved in the high density region and the linearity between v_{20}/v_{22} and L_0 will become better. We have checked that the value of the adjusted coefficient of determination (Adj. R^2) steadily increases from 0.81 at 0.4 GeV/nucleon to 0.93 at 1.2 GeV/nucleon, again indicating that the v_{20}/v_{22} strongly correlates with the slope parameter $L(\rho)$ in the vicinity of ρ_0. It is known from many microscopic many-body theories and phenomenological models that L_0 and K_{sym} are strongly correlated [7,59,60]. Thus, one may suspect that both v_{20}/v_{22} of free protons and v_{20}^n/v_{20}^p are also correlated with K_{sym}. However, after re-plotting Figs. 3 and 4 as a function of K_{sym}, neither of these two observables seem to be distinctly correlated with K_{sym}. For v_{20}/v_{22} of free protons, it seems that both L_0 and K_{sym} can be attributed. On one hand, v_{20}/v_{22} of free protons obtained with Skz4 ($L_0 = 5.8$ MeV, $K_{sym} = -240.9$ MeV) and Skz0 ($L_0 = 35.1$ MeV, $K_{sym} = -242.2$ MeV) which have similar K_{sym} are well separated (see, e.g., Fig. 7). On the other hand, v_{20}/v_{22} obtained with SV-mas08 ($L_0 = 40.2$ MeV, $K_{sym} = -172.4$ MeV) and SLy230a ($L_0 = 44.3$ MeV, $K_{sym} = -98.2$ MeV), for which the different in K_{sym} is about 74 MeV and the difference in L_0 is only about 4 MeV, are not overlapped at higher energies as well. Further calculations with the same L_0 but different K_{sym} (and the same K_{sym} but different L_0) will be certainly required to isolate the contributions from L_0 and K_{sym}.

The result of fitting the excitation function of the v_{20}/v_{22} of free protons is shown in Fig. 7 (b) as a function of the slope L_0. The solid symbols represent the total χ^2 as calculated with the 11 Skyrme interactions. Within a 2-σ uncertainty, the slope is extracted to be $L_0 = 43 \pm 20$ MeV. This result partly covers the $L_0 = 72 \pm 26$ MeV (2-σ uncertainty) obtained from the comparison of the elliptic flow ratio (at mid-rapidities) of neutrons with respect to charged particles with the UrQMD predictions [24], but it is about 30 MeV softer than the result in Ref. [24]. This may originate from the fact that the elliptic flow ratio at mid-rapidity (where higher densities are probed) is used in Ref. [24], while the elliptic flow within a broad range of rapidity (where relatively lower densities are probed) is used in this work.

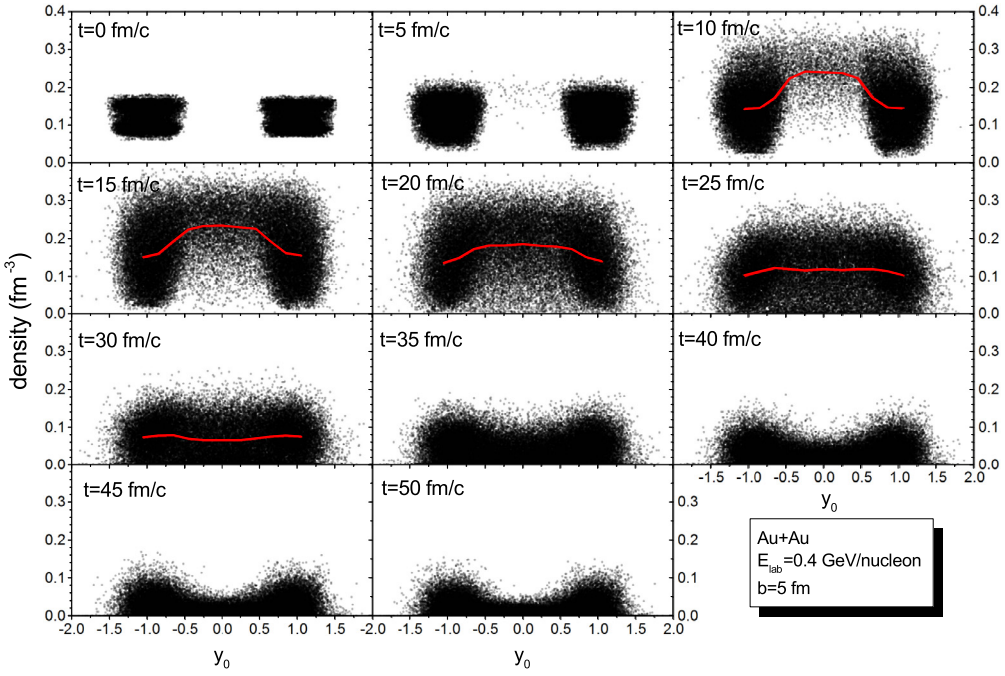

Fig. 5. The nucleon density profile for eleven time steps in Au+Au collision at $E_{\rm lab} = 0.4$ GeV/nucleon with impact parameter $b = 5$ fm. For each time step 100 events are plotted and each nucleon is represented by a circle. The solid lines represent the averaged density for each rapidity bin.

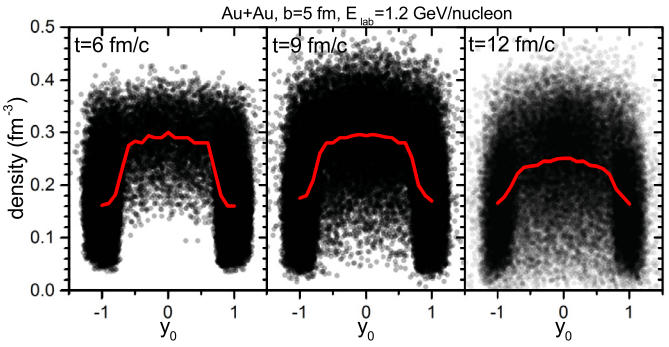

Fig. 6. The same as Fig. 5 but at $E_{\rm lab} = 1.2$ GeV/nucleon.

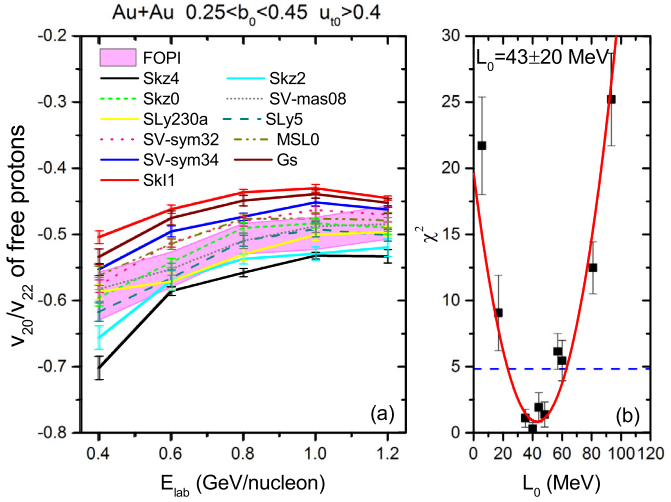

Fig. 7. Left panel: The ratio v_{20}/v_{22} of free protons as a function of beam energy. Lines represent calculations with the selected 11 Skyrme interactions, the shaded band marks the experimental value of the v_{20}/v_{22}. Right panel: The total χ^2 characterizing the fit results obtained with the 11 studied Skyrme forces as a function of the slope parameter L_0. The smooth curve is a quadratic fit to the total χ^2, and the horizontal dashed line is used to determine the error of L_0 within a 2-σ uncertainty.

To summarize, the elliptic flow v_2 of protons as a function of rapidity y_0 in heavy-ion collisions at intermediate energies can be well described by a quadratic fit $v_2 = v_{20} + v_{22} \cdot y_0^2$, and the ratio v_{20}/v_{22} has been found to be sensitive to the density dependence of nuclear symmetry energy. The elliptic flow at mid-rapidity represented by v_{20} carries information on the symmetry energy at high densities, while v_{22} characterizes the flow around target/projectile rapidities where lower density are probed. The slope parameter of the density-dependent symmetry energy is extracted to be $L_0 = 43 \pm 20$ MeV based on the comparison of the FOPI experimental data on the v_{20}/v_{22} of protons with the UrQMD model calculations. The result is comparable with many previous studies on the symmetry energy from nuclear structure properties and also partly overlaps with the result obtained from the elliptic flow ratio of neutrons with respect to charged particles at mid-rapidities reported in Ref. [24]. The result in Ref. [24] is stiffer by about 30 MeV than the result obtained in this work which, to some extent, may arise from the fact that lower densities are probed with the v_{20}/v_{22}. Additional studies of this observable with other model assumptions and/or transport models will be useful for identifying and disentangling remaining systematic uncertainties.

Acknowledgements

We thank Wolfgang Trautmann for a careful reading of the manuscript and valuable communications. The authors acknowledge support by the computing server C3S2 in Huzhou University. The work is supported in part by the National Natural Science Foundation of China (Nos. 11875125, 11947410, 11847315, and 11505057), and the Zhejiang Provincial Natural Science Foundation of China under Grants No. LY18A050002, No. LY19A050001, and the "Ten Thousand Talent Program" of Zhejiang province.

References

[1] B.A. Li, L.W. Chen, C.M. Ko, Phys. Rep. 464 (2008) 113–281.
[2] M.B. Tsang, J.R. Stone, F. Camera, P. Danielewicz, S. Gandolfi, K. Hebeler, C.J. Horowitz, Jenny Lee, W.G. Lynch, Z. Kohley, R. Lemmon, P. Möller, T. Murakami, S. Riordan, X. Roca-Maza, F. Sammarruca, A.W. Steiner, I. Vidaña, S.J. Yennello, Phys. Rev. C 86 (2012) 015803.
[3] M. Baldo, G.F. Burgio, Prog. Part. Nucl. Phys. 91 (2016) 203.
[4] M. Oertel, M. Hempel, T. Klähn, S. Typel, Rev. Mod. Phys. 89 (1) (2017) 015007.
[5] B.A. Li, B.J. Cai, L.W. Chen, J. Xu, Prog. Part. Nucl. Phys. 99 (2018) 29.
[6] X. Roca-Maza, N. Paar, Prog. Part. Nucl. Phys. 101 (2018) 96.
[7] B.A. Li, P.G. Krastev, D.H. Wen, N.B. Zhang, Eur. Phys. J. A 55 (7) (2019) 117.
[8] S. Burrello, M. Colonna, H. Zheng, Front. Phys. 7 (2019) 53.
[9] A. Ono, Prog. Part. Nucl. Phys. 105 (2019) 139.
[10] J. Xu, Prog. Part. Nucl. Phys. 106 (2019) 312.
[11] X. Roca-Maza, M. Brenna, B.K. Agrawal, P.F. Bortignon, G. Colo, L.-G. Cao, N. Paar, D. Vretenar, Phys. Rev. C 87 (2013) 034301.
[12] Z. Zhang, L.W. Chen, Phys. Lett. B 726 (2013) 234.
[13] B.A. Brown, Phys. Rev. Lett. 111 (2013) 232502.
[14] X. Fan, J. Dong, W. Zuo, Phys. Rev. C 89 (2014) 017305.
[15] J.M. Dong, L.J. Wang, W. Zuo, J.Z. Gu, Phys. Rev. C 97 (3) (2018) 034318.
[16] N. Wang, M. Liu, L. Ou, Y. Zhang, Phys. Lett. B 751 (2015) 553.
[17] N.B. Zhang, B.A. Li, Eur. Phys. J. A 55 (2019) 39.
[18] W.J. Xie, B.A. Li, Astrophys. J. 883 (2019) 174.
[19] Z. Xiao, B.A. Li, L.W. Chen, G.C. Yong, M. Zhang, Phys. Rev. Lett. 102 (2009) 062502.
[20] Z.Q. Feng, G.M. Jin, Phys. Lett. B 683 (2010) 140.
[21] P. Russotto, et al., Phys. Lett. B 697 (2011) 471.
[22] M.D. Cozma, Y. Leifels, W. Trautmann, Q. Li, P. Russotto, Phys. Rev. C 88 (4) (2013) 044912.
[23] Y. Wang, C. Guo, Q. Li, H. Zhang, Y. Leifels, W. Trautmann, Phys. Rev. C 89 (2014) 044603.
[24] P. Russotto, et al., Phys. Rev. C 94 (3) (2016) 034608.
[25] P. Danielewicz, P. Singh, J. Lee, Nucl. Phys. A 958 (2017) 147.
[26] L. Lü, H. Yi, Z. Xiao, M. Shao, S. Zhang, G. Xiao, N. Xu, Sci. China, Phys. Mech. Astron. 60 (1) (2017) 012021.
[27] M.D. Cozma, Eur. Phys. J. A 54 (3) (2018) 40.
[28] W. Trautmann, et al., Prog. Part. Nucl. Phys. 62 (2009) 425.
[29] W. Trautmann, et al., Int. J. Mod. Phys. E 19 (08–09) (2010) 1653.
[30] Q. Li, Z. Li, Sci. China, Phys. Mech. Astron. 62 (7) (2019) 972011.
[31] W. Trautmann, AIP Conf. Proc. 2127 (1) (2019) 020003.
[32] P. Danielewicz, R. Lacey, W.G. Lynch, Science 298 (2002) 1592.
[33] C. Sturm, et al., Phys. Rev. Lett. 86 (2001) 39;
C. Fuchs, A. Faessler, E. Zabrodin, Y.-M. Zheng, Phys. Rev. Lett. 86 (2001) 1974;
C. Hartnack, H. Oeschler, J. Aichelin, Phys. Rev. Lett. 96 (2006) 012302.
[34] B.A. Li, L.W. Chen, F.J. Fattoyev, W.G. Newton, C. Xu, J. Phys. Conf. Ser. 413 (2013) 012021.
[35] L.W. Chen, arXiv:1212.0284 [nucl-th].
[36] H. Wolter, PoS Bormio 2012 (2012) 059.
[37] B.A. Li, X. Han, Phys. Lett. B 727 (2013) 276.
[38] Y. Zhang, Z. Li, Phys. Rev. C 74 (2006) 014602.
[39] Y. Wang, C. Guo, Q. Li, H. Zhang, Z. Li, W. Trautmann, Phys. Rev. C 89 (2014) 034606.
[40] J. Aichelin, Phys. Rep. 202 (1991) 233.
[41] B.A. Li, L.W. Chen, Mod. Phys. Lett. A 30 (13) (2015) 1530010.
[42] M. Di Toro, M. Colonna, J. Rizzo, AIP Conf. Proc. 791 (1) (2005) 70.
[43] V. Giordano, M. Colonna, M. Di Toro, V. Greco, J. Rizzo, Phys. Rev. C 81 (2010) 044611.
[44] Z.Q. Feng, Nucl. Phys. A 878 (2012) 3.
[45] C. Guo, Y. Wang, Q. Li, P. Wen, F. Zhang, Phys. Rev. C 91 (2015) 054615.
[46] W.J. Xie, Z.Q. Feng, J. Su, F.S. Zhang, Phys. Rev. C 91 (5) (2015) 054609.
[47] L. Zhang, Y. Gao, Y. Du, G.H. Zuo, G.C. Yong, Eur. Phys. J. A 48 (2012) 30.
[48] W. Reisdorf, et al., FOPI Collaboration, Nucl. Phys. A 848 (2010) 366.
[49] W. Reisdorf, et al., FOPI Collaboration, Nucl. Phys. A 876 (2012) 1.
[50] Y. Wang, C. Guo, Q. Li, A. Le Fèvre, Y. Leifels, W. Trautmann, Phys. Lett. B 778 (2018) 207.
[51] Y. Liu, Y. Wang, Q. Li, L. Liu, Phys. Rev. C 97 (3) (2018) 034602.
[52] Y. Du, Y. Wang, Q. Li, L. Liu, Sci. China, Phys. Mech. Astron. 61 (6) (2018) 062011.
[53] M. Dutra, O. Lourenco, J.S. Sa Martins, A. Delfino, J.R. Stone, P.D. Stevenson, Phys. Rev. C 85 (2012) 035201.
[54] B.A. Li, A.T. Sustich, B. Zhang, Phys. Rev. C 64 (2001) 054604.
[55] P. Danielewicz, Nucl. Phys. A 685 (2001) 368.
[56] J. Xu, L.W. Chen, B.A. Li, H.R. Ma, Astrophys. J. 697 (2009) 1549.
[57] A. Le Fèvre, Y. Leifels, W. Reisdorf, J. Aichelin, C. Hartnack, Nucl. Phys. A 945 (2016) 112.
[58] A. Le Fèvre, Y. Leifels, C. Hartnack, J. Aichelin, Phys. Rev. C 98 (3) (2018) 034901.
[59] P.G. Krastev, B.A. Li, J. Phys. G 46 (7) (2019) 074001.
[60] I. Tews, J.M. Lattimer, A. Ohnishi, E.E. Kolomeitsev, Astrophys. J. 848 (2) (2017) 105.